Indian Society for
Non-Destructive Testing
Hyderabad Chapter

Proc. National Seminar on
Non-Destructive Evaluation
Dec. 7 - 9, 2006, Hyderabad

Lamb Wave Tomographic Reconstruction Using Various MART Algorithms

S. Khare[1], M. Razdan[1], N. Jain[1], P. Munshi[1], B.V. Soma Sekhar[2] and K. Balasubramaniam[2]

[1]Nuclear Engineering & Technology Programme, Indian Institute of Technology, Kanpur-208 016

[2]Centre for Nondestructive Evaluation, Indian Institute of Technology, Chennai-600 036

pmunshi@iitk.ac.in

Abstract

Structural Health Monitoring (SHM) system requires a fast and accurate algorithm for defect detections in the large structures like aircraft skins for which Lamb wave tomography (LWT) appears to be very powerful technique, as their propagation properties depend on the thickness and the mechanical properties of the material. Projection data is collected by electronically scanning an array of ultrasonic sensors arranged in modified crosshole geometry. Extracted energy profile data is used and then final reconstruction is done by various Multiplicative algebraic reconstruction technique (MART) algorithms. Experimental results show that MART is capable of characterizing defects in thin isotropic and composite plates within an error band of $\pm 20\%$.

Keywords: *Lamb waves, Structural health monitoring, Tomographic imaging, MART*

1. Introduction

Structural Health Monitoring has been introduced into the regime of aviation industry as a potential and effective methodology for the assessment of long term deterioration process due to physical aging and routine operation. Ultrasonic Lamb wave testing of plate like structures is of a particular interest in this context to achieve inexpensive and accurate inspection. This requires efficient and cost effective defect detection and characterization methods. Moreover, for real time monitoring the challenge is to scan a large area in a short time span. As guided ultrasonic plate waves with an ability to propagate long distances, Lamb waves [1-6] offer a potentially exciting solution to this problem. Changes in the effective thickness and in material properties caused by surface and subsurface flaws such as disbonds, corrosion, and fatigue cracks can be efficiently detected by measurements of variations in the Lamb wave propagation, these measurements present a highly ill-conditioned system of equation to get reconstructed images. Here, it is shown that MART [7-12] is well suited to reconstruct Lamb wave tomographic data for application to a real time SHM system under limited data conditions.

2. Theory and Formulations

Lamb waves are elastic disturbances propagating in flat plates with traction free surfaces. These are guided waves with an infinite number of modes (in thin plates) which are classified as symmetric and

antisymmetric modes. Specifically it implies that wave motion is symmetric or antisymmetric with respect to the midplane of the plate. Unlike bulk wave modes, all these modes are dispersive.

In case of thin, plate like structures, two factors are to be taken into consideration for in-service inspection using lamb wave tomography. These are: (a) Adopting an appropriate data collection strategy and (b) Fast and reliable reconstruction. A large surface can be rapidly scanned by choosing a data collection geometry which provides maximum angular area coverage of the region of interest. Judicious choice of sensor positions and signal conditioning parameters such as gain and filter cutoffs is also significant for receiving easy to interpret response signals. Here, signal conditioning is required to cut off undesired modes present in the received signal. Received signals are then sampled at a suitable rate, digitized and recorded by a data acquisition system. Computed tomography is then used to quantitatively reconstruct the flaws in the specimen by algebraic reconstruction techniques.

Figure 1 shows the data collection geometry, the axes markers are the sensor positions which are occupied by transceivers. In the present case number of sensors positioned equidistantly on one edge is 11 producing an 11×11 grid. Data is recorded sequentially for all the rays (726 in our case) from all transceivers. Data collection is done by considering six sets of sensor arrangement i.e. left-right, top-bottom, right-top, right- bottom, left-top and left-bottom which give six subsets of equations, for each case we 121 rays hence total 726 rays [13]. Each ray crosses a certain number of cells in its path. The contribution of these rays to different grid elements is given by the weight matrix W_{ij} of dimensions 726×121. For the chosen scanning geometry, the total number of equations in a single crosshole projection equals N^2 equations where, N is the number of sensor positions.

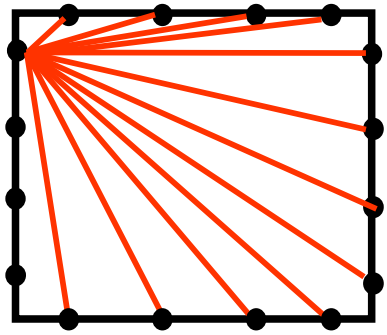

Fig. 1: Modified cross-hole geometry

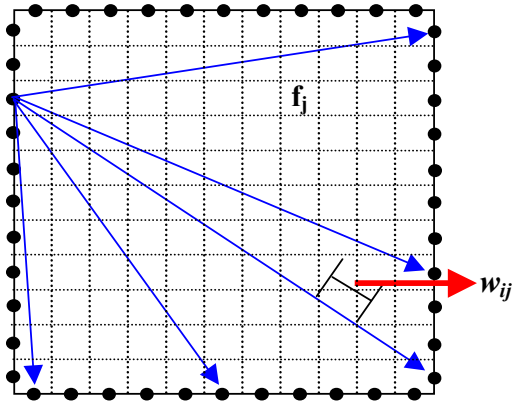

Fig. 2: Cross-borehole Geometry fj is the field value of the j[th] pixel and is the desired image vector. Black dots denote transceivers

To formulate a discretized model, a Cartesian grid of square picture elements (pixels), is introduced into the region that has to be reconstructed (Fig 2). Black dots denote transceivers. The length of intersection of i^{th} ray and j^{th} pixel, denoted by w_{ij} for i=1, 2...M and j=1, 2...N, represents the contribution of j^{th} pixel to the total attenuation along the i^{th} ray and is defined as the weight factor associated with that particular ray-pixel pair. These pixels are numbered following a regular fashion. Thus a weight matrix of dimensions 726x121 is constructed corresponding to 726 rays and 121 pixels. This matrix is calculated once and is provided as an input to the reconstruction algorithm.

The total amplitude of i^{th} ray, denoted by ϕ_i, represents the line integral of the amplitude function along the path of ray. In this discretized model, the line integral

$$\phi_i = \sum_{j=1}^{N} f_j w_{ij} \qquad i = 1, 2, \ldots, M \tag{1}$$

takes the form of finite sum and the model may be described by a system of linear equation, as in matrix notation,

$$\left[W_{ij}\right]\left\{f_j\right\} = \left\{\phi_i\right\} \quad \text{or} \quad A_{ij} x_j = b_i \tag{2}$$

The problem now is the inversion of W_{ij}.

2.1 Reconstruction Algorithm

Three MART algorithms with different corrections have been implemented to reconstruct projection data. The initial approximate projection $\tilde{\phi}_i$ is calculated using Equation (1) with an assumed initial field f^0. MART algorithms considered in the present study are given as:

MART1:

$$\tilde{f}_j^{new} = \tilde{f}_j^{old} \times \prod_{Nc_j} \left[1 - \lambda\left(1 - \frac{\phi_i}{\tilde{\phi}_i}\right)\right]$$

MART2:

$$\tilde{f}_j^{new} = \tilde{f}_j^{old} \times \prod_{Nc_j} \left[1 - \lambda w_{ij}\left(1 - \frac{\phi_i}{\tilde{\phi}_i}\right)\right]$$

MART3: $$\tilde{f}_j^{new} = \tilde{f}_j^{old} \times \prod_{Nc_j} \left[\left(\frac{\phi_i}{\tilde{\phi}_i}\right)\right]^{\lambda w_{ij}}$$

Iterate until

$$\frac{f^{k+1} - f^k}{f^k} \times 100 \le \varepsilon$$

where, ε is the stopping criterion. Inputs to the algorithm are the weight matrix W, projection data matrix ϕ and the initial vector f^0. A MATLAB™ [14] code has been written for the Reconstruction using MART based on above formulation which is also capable of generating the weight matrix for the modified crosshole geometry. Relaxation parameter λ has to play an important role in the iterative tomographic reconstruction techniques. Here it was assumed that if RMS error E_A is at its minimum, in a reconstruction process, then the reconstructed image is with maximum possible features with that particular algorithm. E_A is used to find out the appropriate relaxation parameter.

3. Validation against Simulated data

The performance of the aforementioned algorithms has been checked over simulated data. Mainly two field functions have been used to test performance; constant and impulse, for a square grid of dimensions 11×11 sq. units (Fig. 3). During all reconstructions the initial values in the pixels on the square grid are taken arbitrarily and the pixels simulating flaws are taken to be zero for the purpose of application to a square plate with defected regions.

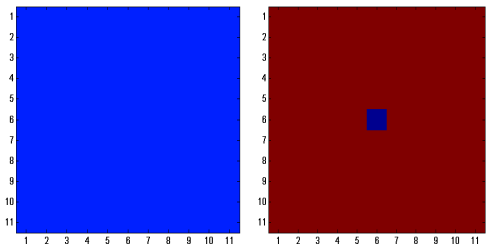

Fig. 3: Simulated specimens Constant field (left), Impulse field (right)

Figure 4 shows the reconstructed constant and impulse fields, for three different MART algorithms. The error is low for constant field, as mentioned above, but algorithms suffer from low value of relaxation parameter (can give limited

features on reconstruction). The error is within tolerable limits for impulse field. Here also relaxation parameter can only have low values but the convergence is better.

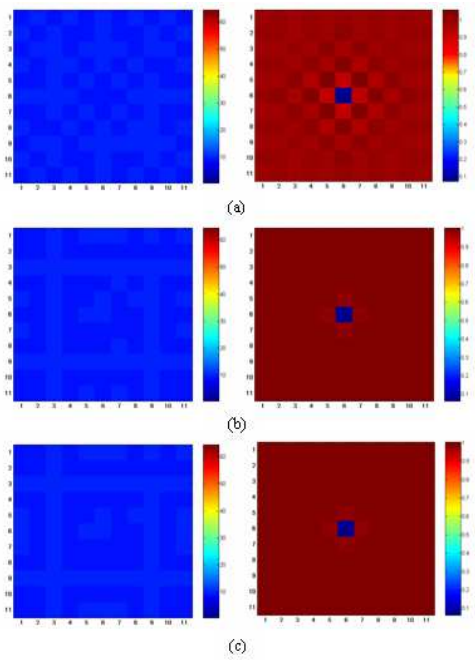

Fig. 4: Reconstructed images constant field (left) and impulse field (right) **(a)** using MART1 **(b)** using MART2 **(c)** using MART3

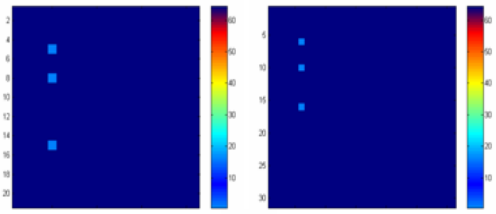

Fig. 5: Reconstruction from simulated projection data for a defective plate. For pixel size **1/21×1/21**, λ=0.01 (left), for pixel size **1/31×1/31**, λ=0.01 (right)

Figure 5 shows the reconstruction from simulated projection data for defective plate for different pixel size. Figure 6 shows variation of RMS error with relaxation parameter in reconstruction for different MART algorithms. Figure 6(a) shows the variation for MART1. For constant field, initially there is a sharp decline in E_A and then it subsidizes as λ is increased. For impulse field, errors are higher for λ values greater than 0.02. Figure 6(b) shows the similar behavior for MART2. However for impulse field, error is higher even for lower values of λ, though its almost constant. For MART3 the behavior is similar to MART2, as shown in Fig. 6(c), though computational time has been substantially reduced. The error is found to be minimum in MART2, although errors in all three cases are comparable. From computational point of view, MART3 has been found to be the fastest of the three algorithms tested here. The various inferences which can be made from this simulation results are as follows.

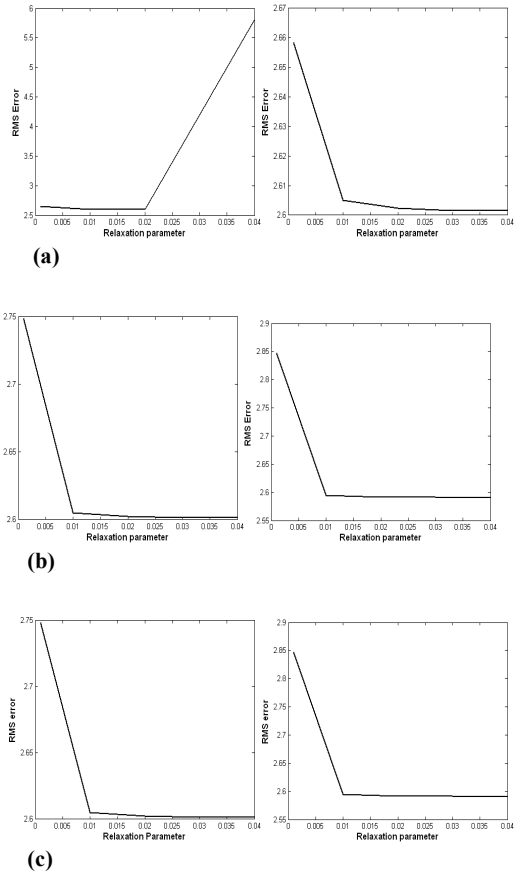

Fig. 6: RMS error vs. relaxation parameter for constant field (left) and impulse field (right) **(a)** MART1 **(b)** MART2 **(c)** MART3

1. The number of iterations decreases as the value of λ increases i.e. cost of all algorithms decreases before divergence as one moves towards higher λ.

2. The low values of λ suggest that the algorithm can reconstruct slow features well.

3. As the number of defects increases, better convergence is achieved for higher values of λ.

4. MART2 shows the best convergence for all values of λ though computational time was higher.

5. MART3 is faster for smaller values of λ but its performance deteriorates for higher values of λ (>0.05).

6. Presently the algorithm works for λ in the range 0-0.05. Beyond that MART does not provide useful results and it diverges.

7. Reconstruction exercise was done for different resolutions. The reconstruction for lowest pixel sizes for which the cost of algorithm is within practical bounds is shown in Fig. 5. The results were very good for small values of λ though computational time will increase with resolution as number of equations to be solved increases.

4. Experiments

The experimental setup consists of a virtual instrument developed on LabView platform, a 32 channel multiplexer, a pulser/receiver and a digitizer interfaced with a Pentium-4 based computer used for instrumentation control and signal conditioning as shown in Fig. 7. The experimental sequence goes from excitation over measurement to data processing. Signal conditioning of response signals has been done to cutoff noise interferences and higher order wave modes in the generated signal. The system was fine tuned to give a good response signal by adjusting gain and filtering parameters. Details of the experimental setup are available elsewhere [13].

The data collection, for each specimen, was done for all six aforementioned transducer configurations. This provided a set of 726 independent measurements. A limited number of sampled values of the received signal were considered to select only lowest order (S_o and A_o) Lamb wave modes. As frequency-thickness product (*fd*) was within 2 MHz-mm for all specimens, observed response was mainly confined to the fundamental modes [4]. Other modes appear in the signal due to mode conversions. These modes being of no interest in the present study are neglected in the sampled domain. Figure 8 shows A-scan images of lamb wave signals through an aluminium plate. The resultant lamb wave was assumed to travel in a straight path, neglecting ray bending. While passing through a flaw (a through-hole in the present case) the wave undergoes attenuation and its amplitude and energy is decreased. Figure 8(a) shows the case when ray passes through a defectless region and Fig 8(b) shows the signal when the ray bypasses the defective region.

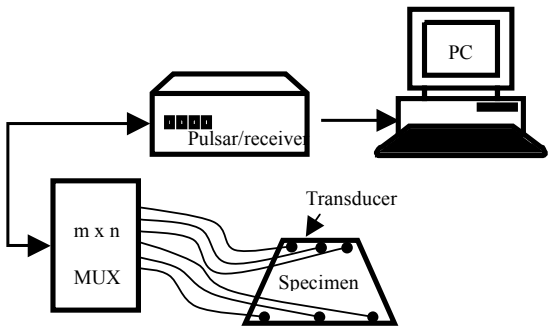

Fig. 7: Schematic of the experimental setup

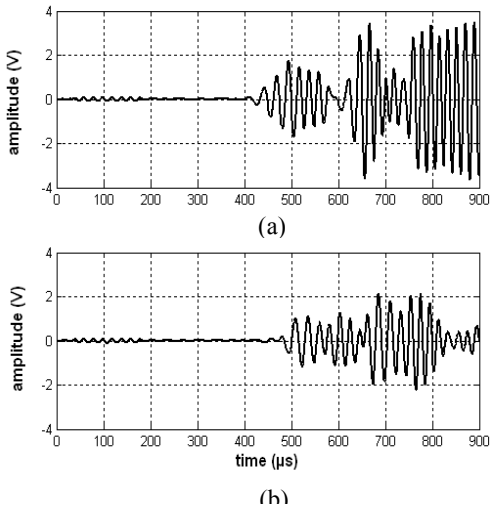

Fig. 8: Lamb wave signal for (a) defectless aluminium plate (b) defective aluminium plate with central hole

There is a distinct change in the amplitude (and thus energy) of the signal. This change in energy is used as a parameter for the reconstruction purpose. Though time of flight is the usual parameter for reconstruction in conventional ultrasonic tomography, its measurement is not as straightforward in the case of Lamb waves due to complexity of the received signals. This has led to the use of energy as the reconstruction parameter.

Experimental data collection was done for different combinations of hole-radius, plate size and thickness. Two different materials were tested, namely isotropic material (aluminium plate) and anisotropic material (Quasi-isotropic (0*n,* 90*n,* 45*m,*-45*m*)*S*, composite plate). The composite used was Carbon fiber reinforced polymer (CFRP). The following three cases were considered for the isotropic aluminum plate:

a) defectless plate (110 mm x 110 mm)

b) defective plate (110 mm x 110 mm) with a through hole in the centre (20 mm dia.)

c) defective plate (300 mm x 300 mm) with off-centered through hole (20 mm dia.)

For Quasi-isotropic CFRP composite plate (thickness 2 mm), the above three cases were repeated.

5. Experimental Results

The projection data collected experimentally was investigated to extract energy information of the traveling waves. The energy data was rearranged in a 726x1 column matrix to serve as an input to the MART algorithm.

Figures 9 and 10 show the images obtained from MART3 algorithm. A high value of the relaxation parameter leads to more rapid convergence, but it was found that under the present circumstances the final outcome of the slowly converging process with a low value of the relaxation parameter (λ) was preferable. Hence a low value of λ (typically 0.1) is used for reconstruction using MART. Output of the algorithm is imaged as reconstructed images

6. Discussion

Specimens of different dimensions are chosen, so as to observe the effect of increasing the scanning area on the traveling lamb waves. In the case of defectless test specimen, data collected had symmetry with respect to ray angle and distance traveled. For the defectless specimen some artifacts do appear but constant density profile is apparent. In case of defective aluminium plate with a through hole in the centre reconstruction using energy data provides good results. The central hole is clearly visible and its orientation does match the sample. The geometry has appeared as a square, instead of a circle because of the large pixel size in the reconstruction.

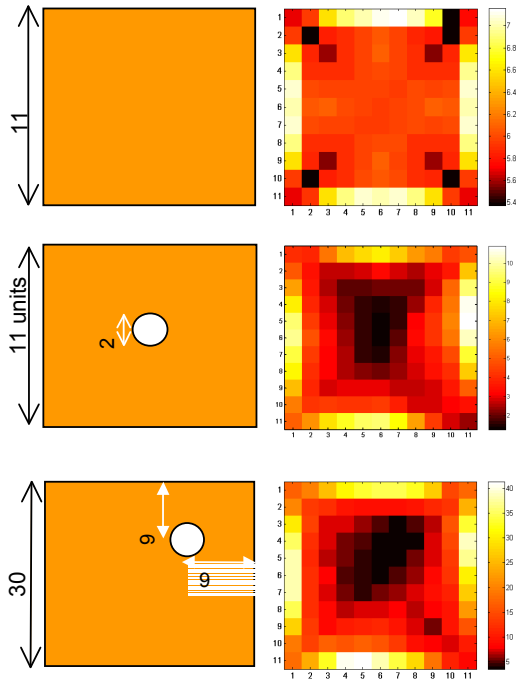

Fig. 9: Schematic and corresponding tomographic reconstruction of an Isotropic Aluminium plate for three test specimens

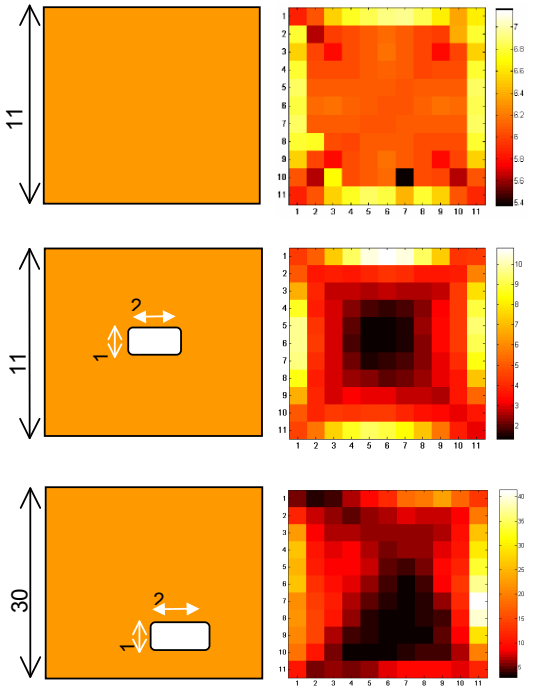

Fig. 10: Schematic and corresponding tomographic reconstruction of a Quasi-isotropic CFRP composite plate for three test specimens

Similar result has been obtained for defective plate with a diagonally off centered defect. Here reconstruction quality is lower than previous two cases. This is because of asymmetry present in the data and increased reflection from edges. The defect location and orientation is correct. However, the defective region has spilled over since the central pixels contribute most to the reconstruction process. This leads to ambiguity in defect sizing. This implies that for detecting defects near the edges, reflection from the rough edges has to be taken into consideration. Also some smoothing technique can be incorporated in the algorithm to temper the "spill-over" effect in case of off-centered defects.

For the defectless composite plate, the constant density cross-section shows up in a fairly uniform way (Fig. 10). This image has a number of artifacts which is expected, as projection data has reduced symmetry due to anisotropy [15] of the material. In case of centrally defected composite plate the central hole is clearly visible and its orientation matches that of the sample. Anisotropy has again affected the visual quality of reconstructed images in the form of artifacts. In case of off-centered defect the defect location is clearly identified. Here also, the defective region has spilled over to the centre. To improve image quality for the composite case material anisotropy also has to be taken into consideration besides other factors like reflection and smoothing.

7. Conclusions

MART3 algorithm has provided encouraging results and is found suitable for reconstruction of Lamb wave tomographic data. Results are good for isotropic case. For composite material (CFRP), defects are clearly identifiable with correct location and orientation information. Image quality is affected due to appearance of artifacts, which can be attributed to various factors

such as reflection from edges, ray bending and scattering. In case of composite materials effect of material anisotropy has to be taken into account for improved reconstruction.

8. References

1. Chang F. K., Proceedings of the 2nd International Workshop on Structural Health Monitoring, September, 8-10, Stanford, CA (1999).
2. Schwarz W. G., Read M. E., Kremer M. J., Hinders M. K. and Smith B. T., SPIE Conference on Nondestructive Evaluation of Aging Aircraft, Airports, and Aerospace Hardware III SPIE Vol. 3586, 292 (1999).
3. Viktorov A., Rayleigh and Lamb waves, Plenum Press, New York (1970).
4. Rose J. L., Ultrasonics waves in solid media, University Press, Cambridge (1999).
5. Krautkramer J. and Krautkramer H., Ultrasonic testing of materials, Springer-Verlag (1983).
6. Alleyne D. N. and Cawley P., Proceedings of the Institution of Mechanical Engineers, ProQuest Science Journals p. 217-226 (1996).
7. Kak A. C. and Slaney M., Principles of Computerized Tomographic Imaging. IEEE press (1998).
8. Herman G. T., Image Reconstruction from Projections: The fundamentals of Computerized Tomography, Academic Publishers, New York (1980).
9. Subbarao P., Munshi P. and Muralidhar K., NDT & E International, 30(6), 359-370 (1997).
10. Gordon R., Bender R. and Herman G. T. J. Theo. Biol. 29, 471-481 (1970).
11. R. Gordon, G. T. Herman. Int. Rev. Cytol, 38, 111-115 (1974).
12. Lent A., "A convergent algorithm for maximum entropy image reconstruction with a medical X-ray application", Proc. SPIE Image Analysis and Evaluation, R. Shaw, ed, 249-257 (1977).
13. Malyarenko E. V. and Hinders M. K., J., Acoustical Society of America 108 (October), 1631-1639 (2000).
14. MATLAB documentation available at www.mathworks.com
15. Guo N. and Cawley P., "The interaction of lamb waves with delaminations in composite laminates", NDT & E international, 29 (4) (1996).